ELSEVIER

Thermochimica Acta 344 (2000) 103–117

thermochimica acta

www.elsevier.com/locate/tca

Activation energies for thermal ionic and neutral desorptions from thin films of lithium halides

Hiroyuki Kawano*, Yongfa Zhu[1], Takanori Maeda, Shûji Sugimoto

Department of Chemistry, Faculty of Science, Ehime University, Matsuyama 790-8577, Japan

Aaccepted 23 August 1999

Abstract

To clarify the mechanism of positive-ionic and neutral desorptions from heated lithium halide (LiX, X = F, Cl, Br or I), a small amount (approx. 10^{-12}–10^{-7} mol) of LiX was deposited on a platinum plate (ca. 0.03–0.04 cm^2) to prepare a thin film ($\theta_0 = 10^{-1}$–10^3 molecular layers at the start), and it was heated up to ca. 1500 K at a constant rate ($\beta = 0.4$–140 K/s) in vacuum (approx. 10^{-4} Pa) using our dual-ion source system which made it possible to measure simultaneously the desorption rates (D^0 and D^+) of neutral molecule (LiX^0) and ion (Li^+). The temperature-programmed desorption spectra thus obtained were different in pattern from that observed previously with NaX where each of NaX^0 and Na^+ had only one peak. Namely, the high peaks (P_1^0 and P_2^+) of LiX^0 and Li^+ appeared at a temperature generally lower and higher than the melting point (T_m) of each LiX, respectively, while low peaks (P_1^+, P_2^0, P_3^0 and P_3^+) appeared usually above T_m. Theoretical analysis of the β-dependence of peak appearance temperatures yields the activation energies (E_1^{0+}–E_3^{0+}) for desorption of LiX^0 (or Li^+) giving $P_1^{0+}-P_3^{0+}$, respectively, and also the frequency factors (ν_1^{0+}–ν_2^{0+}) corresponding to respective peaks. With respect to LiF ($\theta_0 \approx 13$ molecular layers), for example, E_1^0 and E_1^+ were 220 and 167 kJ/mol, respectively, while ν_1^0 and ν_1^+ were respectively 1×10^{17} and 8×10^{10}/s. In conclusion, (1) each desorption obeys the first-order kinetics, (2) $P_1^0-P_3^0$ originate from the desorption from LiX at the state of physical adsorption, crystal or chemisorption, (3) $P_1^+-P_3^+$ are due to the desorption from active sites (high work function sites; e.g., 724 kJ/mol for LiC1) on the heterogeneous surface of LiX itself or Pt, and (4) the ionization efficiency (D^+/D^0) even at $P_1^+-P_3^+$ is usually less than 1% mainly because the fraction of the active sites is less than 1% of the desorbing surface area.

Keywords: Activation energy; Lithium halide films; Frequency factor; Ionic and neutral desorption rates; Work function

1. Introduction

By using our dual-ion source connected with a temperature-programmed heating system [1,2], we have been studying the thermal desorption of both positive ion (M^+) and neutral molecule (MX^0) from a film of alkali halide (MX) deposited on a metal surface (ca. 10^{-2} cm^2 in sample coating area) heated up to ca. 1500 K in vacuum (ca. 10^{-4} Pa). Up to date, the desorption rates (D^+ and D^0) of M^+ and MX^0 have been measured as a function of sample temperature (T) increased at a constant rate ($\beta \approx 10^{-1}-10^2$ K/s) or the initial film thickness ($\theta_0 \approx 10^{-1}-10^4$ molecular layers) of NaC1, NaBr, NaI, RbC1 or LiC1, and both activation energies (E^+ and E^0) and frequency factors

* Corresponding author. Fax: +81-89-9279590.
E-mail address: kawano@dpc.ehime-u.ac.jp (H. Kawano).
[1] Present address: Department of Chemistry, Tsinghua University, Beijing 100084, People's Republic of China.

0040-6031/00/$ – see front matter
PII: S0040-6031(99)00333-0

(ν^+ and ν^0) have been determined with each sample [3–5]. In the present work, four species of lithium halides (LiX) have been employed as samples to obtain further information about the desorption, thereby yielding that each of Li^+ and LiX^0 has two or three peaks in contrast to each of Na^+ and NaX^0 having only one peak at a temperature above or below the melting point of NaX [2,3].

This paper summarizes the data on D^{0+}, E^{0+} and ν^{0+} together with the work function (ϕ^+) effective for the desorption of Li^+ from each LiX and also discusses the mechanism of ionic and neutral desorptions from LiX.

2. Experimental method

A schematic diagram of the dual-ion source [2] is shown in Fig. 1, where F_1, F_2 and G are the platinum plate (0.03–0.04 cm^2 in surface area), a coiled platinum wire (0.02 cm in diameter and 4 cm in total length) and grid wires for retarding the ions desorbed from F_1 or F_2. With regard to the earth, F_1, F_2 and G were held at +16, +50 and +30 V, respectively. With a hypodermic microsyringe, a definite volume (typically 1.00 μl) of an aqueous solution (10^{-5}–10^{-1} mol/l) of LiX (above 99.9% in purity) was transferred to F_1, thereby preparing a thin film ($\theta_0 \approx 10^{-1}$–10^3 molecular layers at the start).

In a high vacuum (ca. 10^{-4} Pa) attained with an oil diffusion pump system with a liquid nitrogen trap, F_1 was heated with a coiled rhenium wire (H, 0.02 cm in diameter and 4 cm in total length) up to ca. 1500 K at a constant heating rate ($\beta \approx 0.4$–140 K/s) using a temperature controller. The sample temperature (T) was monitored with a calibrated alumel–chromel thermocouple (A). A part of the neutral molecules (LiX^0) evaporating from F_1 was directed onto F_2 (usually kept at ca. 1200 K), from which Li^+ was emitted after surface ionization [6,7] of LiX^0. The primary and secondary positive ion currents (i_1^+ and i_2^+) of Li^+ thus desorbed from F_1 and F_2 were directly collected with Faraday cups of C_1 and C_2, respectively, and recorded with a microcomputer system. The efficiencies (η^+ and η^0) of the primary ion collection by C_1 and of the secondary ion collection by C_2 after surface ionization of LiX^0 were usually 0.34 ± 0.02 and typically ca. 10^{-6}, respectively, which were determined by our simple method [1].

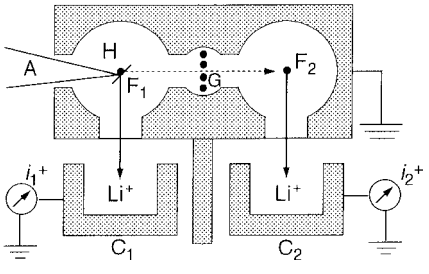

Fig. 1. Dual-ion source system developed in our laboratory.

A typical spectrum of the temperature-programmed desorption (TPD) from LiF is shown in Fig. 2, where the initial sample amount and thickness (N_0 and θ_0) are 6.02×10^{15} molecules and 128 molecular layers (ML), respectively, and β is 3.4 K/s. The current of i_1^+ has two peaks (P_1^+ and P_2^+) at the temperatures ($T_{P_1}^+$ and $T_{P_2}^+$) of 861 and 1162 K, respectively, while i_2^+

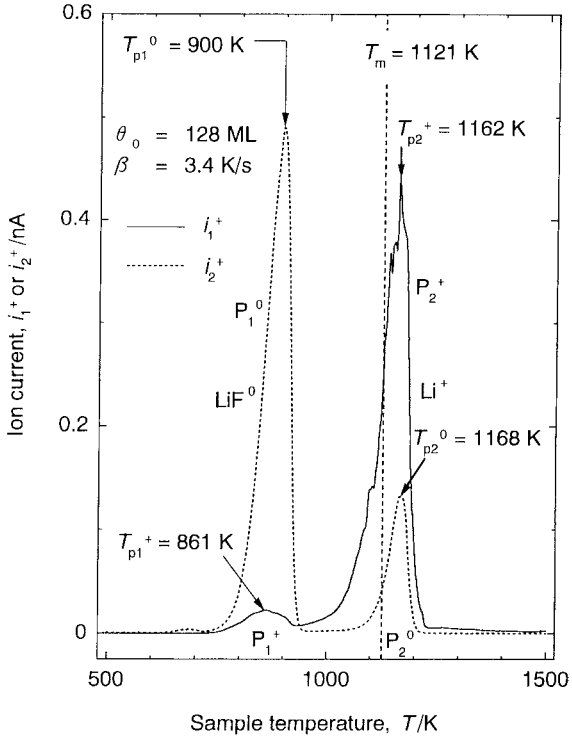

Fig. 2. Typical spectrum obtained with LiF ($\theta_0 = 128$ ML) at $\beta = 3.4$ K/s. For further information, see row 4 in Table 1.

shows P_1^0 at $T_{P_1}^0 = 900$ K and P_2^0 at $T_{P_2}^0 = 1168$ K. It should be noted that both $T_{P_2}^+$ and $T_{P_2}^0$ are higher than the melting point ($T_m = 1121$ K) of LiF.

The numbers of Li^+ and LiX^0 desorbed from F_1 per second are readily evaluated from

$$n^+ = i_1^+/e\eta^+ \text{ ions/s}, \quad (1)$$

and

$$n^0 = i_2^+/e\eta^0 \text{ molecules/s}, \quad (2)$$

where e is the elementary electric charge. The amount (N) and the mean film thickness (θ) of the sample remaining on F_1 at a given time (t) after starting the programmed heating are calculated from

$$N = N_0 - \sum n^+ t - \sum n^0 t, \quad (3)$$

and

$$\theta = \frac{L^2 N}{2S}. \quad (4)$$

Here, L is the lattice constant of LiX, ranging from 4.01×10^{-8} to 6.01×10^{-8} cm, and S is the surface area (0.0340–0.0425 cm^2) of F_1. Therefore, the monolayer (θ_1) of LiX on F_1 corresponds to $N_1 = 2S/L^2$ molecules. Even at $\theta \approx 5$ ML, however, a part of the surface of F_1 may be left below 1 ML because the surface roughness factor of F_1 is generally larger than unity and also because the thickness of sample layers prepared from any aqueous solution is usually far from uniformity.

In this way, we measured the absolute (not relative) values of (1) the layer desorption rates ($D^{0+} \equiv n^{0+}/\theta_1$ ML/s) of LiX^0 or Li^+, (2) the ionization efficiency ($\varepsilon^+ \equiv n^+/(n^0 + n^+) \approx n^+/n^0 = D^+/D^0$) of LiX and also (3) both N and θ of LiX remaining on F_1 at a given time (t) and hence at a given temperature (T).

3. Results and discussions

3.1. TPD spectra

Firstly, the effect of initial film thickness (θ_0) upon a TPD spectrum was examined with LiF with β fixed at 3.4 K/s. The results thus obtained are shown in Fig. 3 and Table 1. As θ_0 increases from 0.13 to 1280 ML, (1) the appearance temperature ($T_{P_1}^0$) of P_1^0, for example,

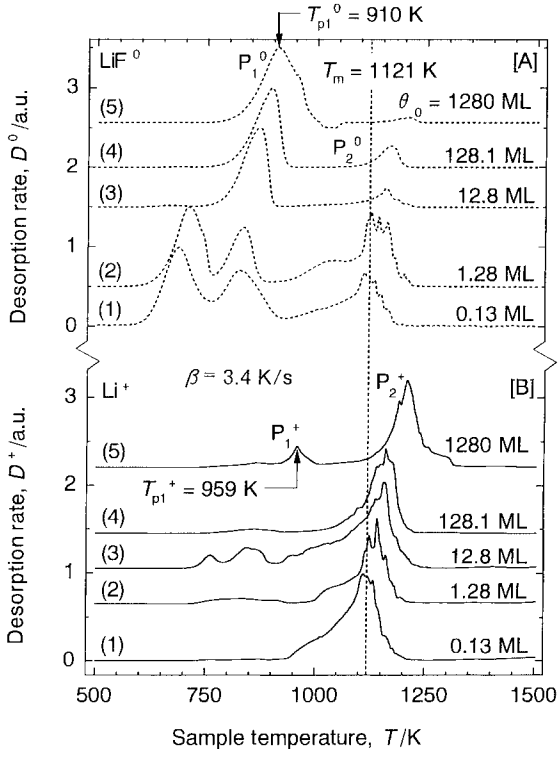

Fig. 3. TPD spectra of LiF^0 and Li^+ desorbed from various values of thickness ($\theta_0 = 0.13$–1280 ML) of LiF at a common heating rate ($\beta = 3.4$ K/s). For further information, see Table 1.

shifts from 826 to 910 K, (2) the film thickness ($\theta_{P_1}^0$) at $T_{P_1}^0$ increases from 0.07 to 684 ML, and (3) the desorption rate ($D_{P_1}^0$) expressing the height of P_1^0 increases from 0.001 to 36.6 ML/s. A similar tendency is found with both $T_{P_1}^+$ and $D_{P_1}^+$, too, although the ionization efficiency ($\varepsilon_{P_1}^+$) at $T_{P_1}^+$ decreases from ca. 10^{-4} to 10^{-7} with an increase in θ_0

Secondly, the effect of heating rate (β) was studied with LiF at $\theta_0 = 128$ ML, thereby yielding the results summarized in Fig. 4 and Table 2. With an increase in β from 3.4 to 139.6 K/s, (1) $T_{P_1}^0$ and $T_{P_1}^+$ increase from 900 to 981 K and 861 to 986 K, respectively, (2) $D_{P_1}^0$ and $D_{P_1}^+$ also increases from 5.17 to 73.6 ML/s and from 0.088×10^{-4} to 21.4×10^{-4} ML/s, respectively, but (3) $\varepsilon_{P_1}^+$ does not monotonically increase. Such a complicated dependence upon β is observed with $D_{P_2}^0$ and $D_{P_2}^+$ and $\varepsilon_{P_2}^+$, too.

The same examination was made with LiC1, LiBr and LiI, thus yielding Figs. 5–10 and Tables 3–5.

Table 1
Summary of the data obtained as a function of the initial amount (N_0) or layer thickness (θ_0) of LiF ($T_m = 1121$ K) deposited on a platinum surface (see Fig. 3) (the heating rate (β) is about 3.4 K/s)

Curve (Fig. 3)	N_0 (molecules)	θ_0 (ML)	T_P^0 (K)		T_P^+ (K)		θ_P^0 (ML)		θ_P^+ (ML)		D_P^0 (ML s^{-1})		D_P^+ ($\times 10^{-4}$ ML s^{-1})		$\varepsilon_P^+(\times 10^{-4})$	
			P_1^0	P_2^0	P_1^+	P_2^+	P_1^0	P_2^0	P_1^+	P_2^+	P_1^0	P_2^0	P_1^+	P_2^+	P_1^+	P_2^+
1	6.02×10^{12}	0.13	826	1114	–	1113	0.07	0.02	–	0.02	0.001	0.001	–	0.44	–	370
2	6.02×10^{13}	1.28	834	1140	834	1140	0.72	0.18	0.72	0.18	0.015	0.018	0.021	0.34	1.45	19.4
3	6.02×10^{14}	12.8	870	1160	851	1159	5.42	2.34	8.14	2.34	0.011	0.125	0.087	0.36	0.19	2.89
4	6.02×10^{15}	128	900	1168	861	1162	52.6	8.23	97.1	10.70	5.17	1.41	0.088	1.73	0.027	1.24
5	6.02×10^{16}	1280	910	1210	959	1209	684	40.0	273	42.6	36.6	8.61	0.133	0.55	0.006	0.062

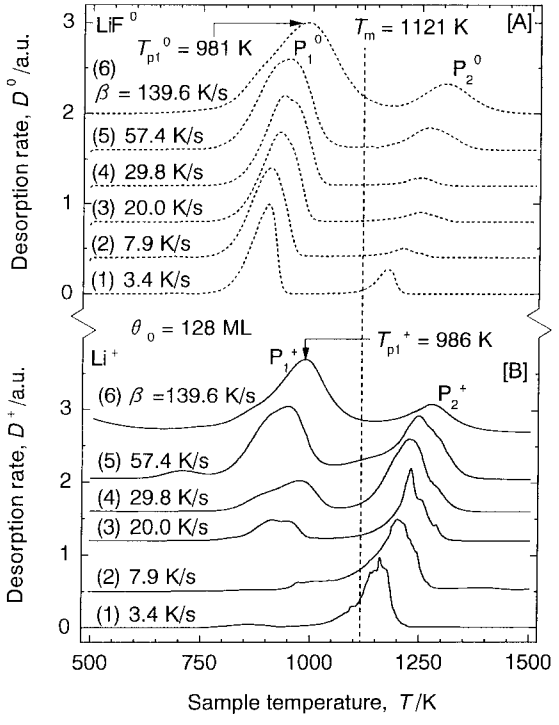

Fig. 4. Spectra observed with LiF ($\theta_0 = 128$ ML) at various heating rates (see Table 2).

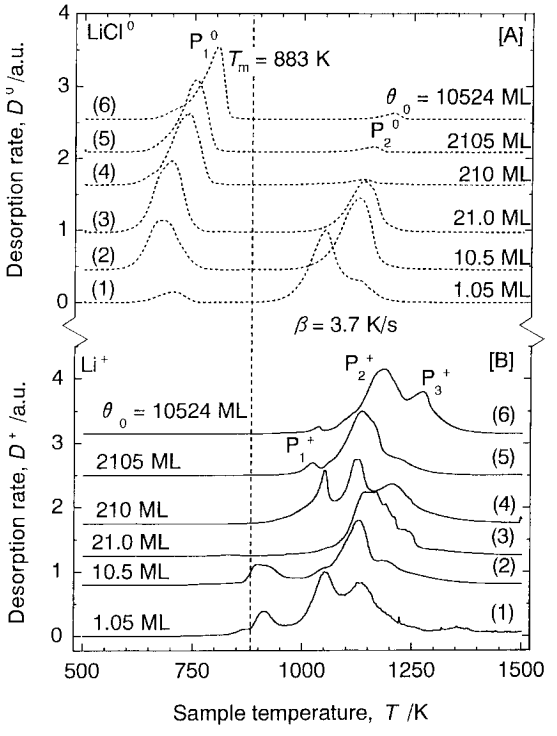

Fig. 5. Spectra of $LiC1^0$ and Li^+ at $\beta = 3.7$ K/s (see Table 3).

Compared with LiF, LiI is roughly the same in pattern of TPD spectrum, but LiC1 and LiBr have the additional peaks of P_3^+ and P_3^0, respectively. In any sample, however, it is common that P_1^0 appears below T_m while P_2^0–P_3^0 and P_2^+–P_3^+ exist above T_m. It should be noted that LiF alone yields P_1^+ at a low temperature below T_m. These results suggest that Li^+ can be desorbed under a special condition alone, as will be discussed below.

3.2. Activation energy and frequency factor

The data on T_P^0 and T_P^+ determined with LiF as a function of β (see Fig. 4 and Table 2) lead to Fig. 11,

Table 2
Summary of the data achieved as a function of the rate (β) heating LiF deposited on a surface of Pt (see Fig. 4)[a]

Curve (Fig. 4)	β (Ks^{-1})	η^0 ($\times 10^{-6}$)	T_P^0 (K)		T_P^+ (K)		θ_P^0 (ML)		θ_P^+ (ML)		D_P^0 (ML s^{-1})		D_P^+ ($\times 10^{-4}$ ML s^{-1})		ε_P^+ ($\times 10^{-4}$)	
			P_1^0	P_2^0	P_1^+	P_2^+	P_1^0	P_2^0	P_1^+	P_2^+	P_1^0	P_2^0	P_1^+	P_2^+	P_1^+	P_2^+
1	3.4	12.5	900	1168	861	1162	52.6	8.23	97.1	10.7	5.17	1.41	0.088	1.73	0.027	1.24
2	7.9	8.58	905	1203	–	1203	51.0	5.08	–	5.1	9.40	0.97	–	1.33	–	1.37
3	20.0	3.57	922	1239	929	1231	62.0	5.92	54.6	6.9	22.6	2.38	1.57	5.82	0.071	0.93
4	29.8	4.54	935	1247	937	1233	70.8	11.1	69.2	14.1	24.7	7.44	1.57	7.12	0.064	1.00
5	57.4	5.66	943	1262	948	1249	65.3	11.6	61.2	14.1	42.1	10.4	7.98	6.99	0.191	0.70
6	139.6	1.39	981	1297	986	1276	71.2	13.3	68.6	17.3	73.6	24.2	21.4	8.17	0.291	0.37

[a]The sample amount (N_0) and thickness (θ_0) at the start are 6.02×10^{15} molecules and 128 molecular layers (ML), respectively.

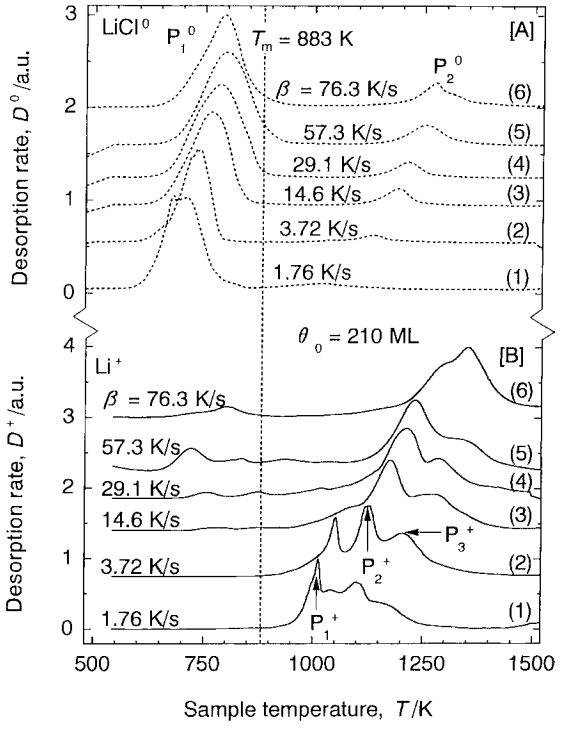

Fig. 6. Spectra achieved with LiC1 at $\theta_0 = 210$ ML (see Table 3).

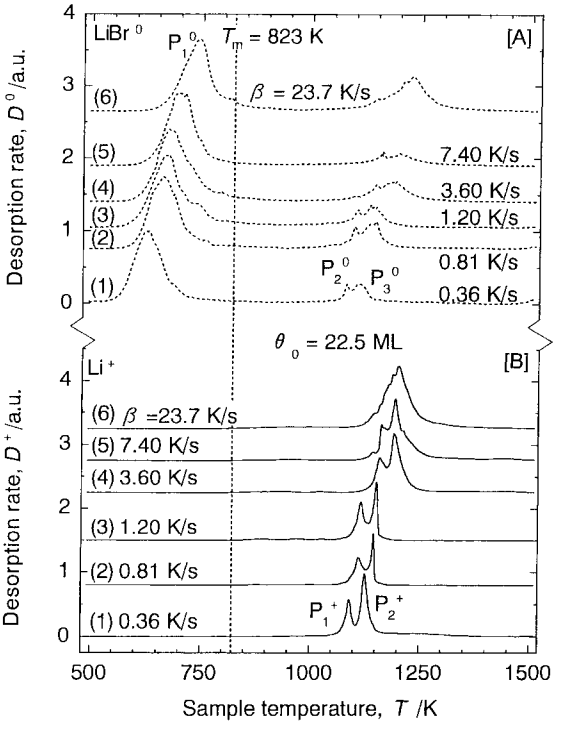

Fig. 8. Spectra observed with LiBr at $\theta_0 = 22.5$ ML (see Table 4).

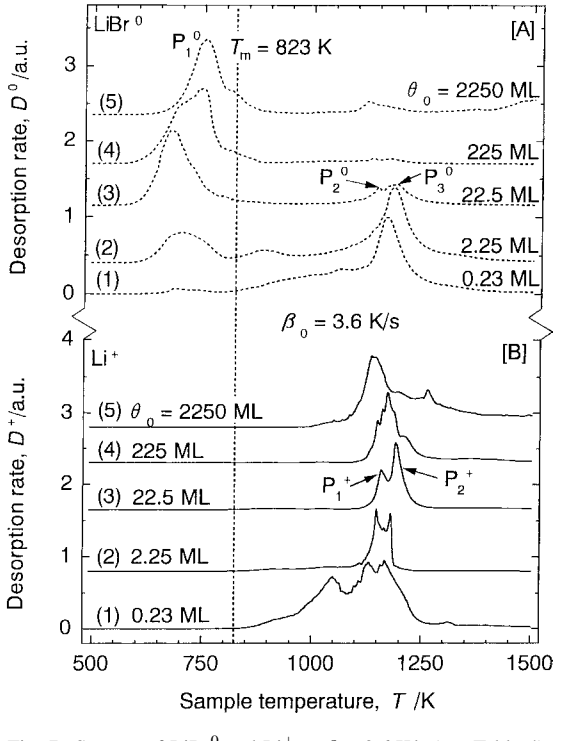

Fig. 7. Spectra of LiBr^0 and Li$^+$ at $\beta = 3.6$ K/s (see Table 4).

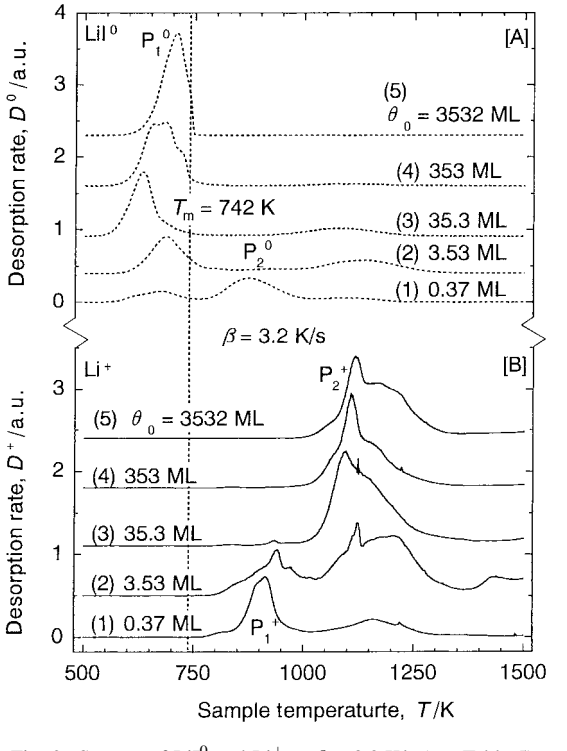

Fig. 9. Spectra of LiI^0 and Li$^+$ at $\beta = 3.2$ K/s (see Table 5).

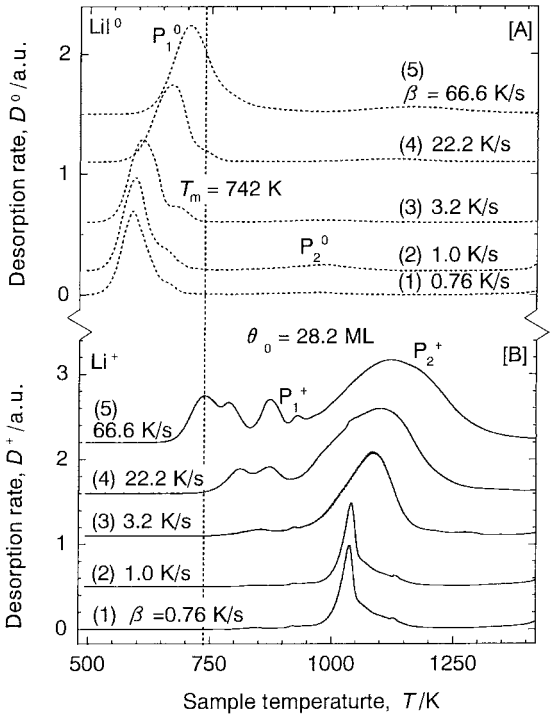

Fig. 10. Spectra obtained with LiI at $\theta_0 = 28.2$ ML (see Table 5).

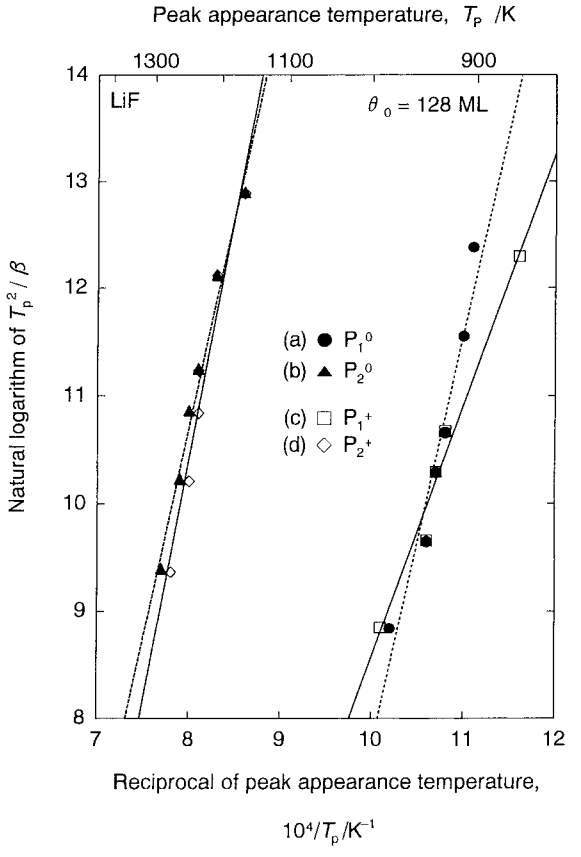

Fig. 11. Reciprocal of the peak appearance temperature (T_P) vs. the natural logarithm of T_P^2/β measured with LiF at $\theta_0 = 128$ ML (see row 2 in Table 6).

indicating that all the lines are well expressed by Eq. (5) [8] and hence that each desorption arises from the first-order process.

$$\ln\left(\frac{T_P^2}{\beta}\right) = \frac{E}{RT_P} - \ln\left(\frac{\nu R}{E}\right). \quad (5)$$

Here, E and ν are the activation energy and the frequency factor for each desorption, respectively, while R is the gas constant. The values of E and ν determined from the slope and the intercept of each line in Fig. 11 are summarized in Table 6, where E_s^0 is the sublimation heat of bulk LiX at temperatures around $T_{P_1}^0$, readily evaluated from thermochemical tables [9]. In the case of LiF at $\theta_0 = 12.8$ ML, for example, $E_1^0 = 220$ kJ/mol is smaller than $E_s^0 = 270$ kJ/mol, strongly suggesting that LiF is desorbed from physical adsorption state rather than crystal state because θ_0 is as small as 12.8 ML. At $\theta_0 = 128$ ML, on the other hand, $E_1^0 = 281$ kJ/mol is nearly the same with E_s^0 within the experimental error of about ±4%, showing that P_0^1 originates mainly from crystal sublimation. In the case of LiC1, E_1^0 increases from 135 to 145 kJ/mol as θ_0 increases from 20.4 to 210 ML. At $\theta_0 = 2105$ ML, E_1^0 becomes 205 kJ/mol, exactly the same with E_s^0. This result indicates that P_1^0 shown by curve 5 of Fig. 5A is due to sublimation not from physical adsorption state but from crystal state of LiC1 at temperatures much below T_m (883 K). Both LiBr and LiI starting at $\theta_0 = 22.5$ and 28.2 ML, respectively, show that E_1^0 is lower by about 50 kJ/mol than E_s^0 and hence suggest that any P_1^0 in Figs. 7–10 is due to desorption from physical adsorption state. On the other hand, E_2^0 and E_3^0 found with LiBr are much larger than E_s^0, strongly suggesting that P_2^0 and P_3^0 originate from the respective chemical adsorption states.

When Li^+ is desorbed from a catalytic metal surface at $\theta < 10^{-2}$ ML (virtually clean surface), E^+ is

Table 3
Summary of the data on LiC1 ($T_m = 883$ K) (see Figs. 5 and 6)

Curve	N^0 (molecules)	η^0 (10^{-6})	θ_0 (ML)	β (Ks^{-1})	T_P^0 (K)		T_P^+ (K)			θ_P^0 (ML)		θ_P^+ (ML)			D_P^0 (ML s^{-1})		D_P^+ ($\times 10^{-4}$ ML s^{-1})			ε_P^+ ($\times 10^{-4}$)		
					P_1^0	P_2^0	P_1^+	P_2^+	P_3^+	P_1^0	P_2^0	P_1^+	P_2^+	P_3^+	P_1^0	P_2^0	P_1^+	P_2^+	P_3^+	P_1^+	P_2^+	P_3^+
Fig. 5																						
1	3.01×13^{13}	–	1.05	3.7	705	1050	914	1054	1132	0.98	0.51	0.94	0.49	0.11	0.005	0.04	0.076	0.19	0.16	120	5.4	15
2	3.01×10^{14}	–	10.5	3.7	677	1128	907	1130	1186	8.6	2.5	6.5	2.4	0.27	0.18	0.26	0.37	1.2	0.46	150	4.7	20
3	6.02×10^{14}	–	21.0	3.7	698	1138	–	1154	–	14.4	9.4	–	2.6	–	0.55	0.40	–	1.1	–	–	3.0	–
4	6.02×10^{15}	–	210	3.7	734	1136	1054	1126	1206	96.4	11.3	21	13	3.9	8.8	0.71	3.9	4.8	2.9	18	7.1	16
5	6.02×10^{16}	–	2105	3.7	754	1158	1023	1138	1215	854	47.5	147	87	7.2	100	7.5	1.1	5.6	1.5	3.3	0.95	58
6	3.01×10^{17}	–	10524	3.7	804	1205	1036	1184	1276	3075	233	787	490	14	561	48	3.5	30	20	5.5	0.90	16
Fig. 6																						
1	6.02×10^{15}	13.8	210	1.76	699	1010	1014	1042	1100	117	11.5	11	8.0	3.6	3.2	0.19	3.4	2.0	2.3	17	11	24
2	6.02×10^{15}	4.0	210	3.72	734	1136	1054	1126	1206	96.4	11.3	21	13	3.9	8.8	0.71	3.9	4.8	2.9	18	7.1	16
3	6.02×10^{15}	4.7	210	14.6	766	1193	1080	1177	1265	107	11.6	27	17	1.7	25	4.5	0.65	2.0	1.0	2.0	0.52	2.1
4	6.02×10^{15}	1.4	210	29.1	781	1211	–	1198	1301	110	11.8	–	15	1.7	44	7.3	–	1.6	0.88	–	0.25	0.97
5	6.02×10^{15}	0.32	210	57.3	795	1254	–	1234	1329	120	17.1	–	23	3.5	81	17	–	1.9	0.88	–	0.13	0.22
6	6.02×10^{15}	0.16	210	76.3	794	1278	–	1294	1351	123	25.9	–	21	9.7	106	29	–	1.5	2.0	–	0.08	0.25

Table 4
Data obtained with LiBr ($T_m = 823$ K) (see Figs. 7 and 8)

Curve	N_0 (molecules)	η^0 ($\times 10^{-6}$)	θ_0 (ML)	β (K s^{-1})	T_P^0 (K)			T_P^+ (K)		θ_P^0 (ML)			θ_P^+ (ML)			D_P^0 (ML s^{-1})		D_P^+ ($\times 10^{-4}$ ML s^{-1})		ε_P^+ ($\times 10^{-4}$)	
					P_1^0	P_2^0	P_3^0	P_1^+	P_2^+	P_1^0	P_2^0	P_3^0	P_1^+	P_2^+	P_1^0	P_2^0	P_3^0	P_1^+	P_2^+	P_1^+	P_2^+
Fig. 7																					
1	6.02×10^{12}	–	0.23	3.6	682	1068	1168	1133	1170	0.22	0.15	0.08	0.11	0.07	0.0003	0.0013	0.004	8.07	7.34	3050	1839
2	6.02×10^{13}	–	2.25	3.6	700	1139	1182	1149	1182	1.99	1.05	0.68	0.99	0.67	0.016	0.0191	0.042	25.6	22.6	930	534
3	6.02×10^{14}	–	22.5	3.6	677	1147	1184	1159	1191	15.8	4.21	2.73	3.76	2.43	0.59	0.147	0.16	24.7	43.5	205	272
4	6.02×10^{15}	–	225	3.6	725	1134	1180	1174	1211	123	13.5	8.51	9.26	5.99	5.5	0.509	0.42	45.0	17.0	108	79
5	6.0×10^{16}	–	2250	3.6	753	1124	1165	1143	1198	1507	551	460	504	40.7	57.9	10.8	7.54	14.1	7.22	1.7	1.5
Fig. 8																					
1	6.02×10^{14}	4.64	22.5	0.36	626	1082	1112	1090	1128	15.2	4.1	2.8	3.8	2.1	0.07	0.019	0.018	3.9	6.5	295	557
2	6.02×10^{14}	4.76	22.5	0.81	662	1098	1139	1112	1147	15.3	5.1	3.1	4.5	2.5	0.14	0.047	0.050	7.6	16	235	299
3	6.02×10^{14}	5.84	22.5	1.20	671	1104	1141	1117	1155	15.0	3.6	2.2	3.2	1.6	0.21	0.050	0.060	10	16	270	369
4	6.02×10^{14}	6.34	22.5	3.60	677	1148	1184	1159	1191	15.8	4.2	2.7	3.8	2.4	0.60	0.15	0.16	25	43	205	272
5	6.02×10^{14}	7.64	22.5	7.40	699	1163	1201	1164	1195	14.1	3.3	2.2	3.3	2.4	1.44	0.27	0.24	47	76	195	332
6	6.02×10^{14}	3.01	22.5	23.7	740	–	1228	–	1201	15.1	–	3.6	–	5.3	3.71	–	1.84	–	88	–	69.7

Table 5
Data on LiI ($T_m = 742$ K) (see Figs. 9 and 10)

Curve	N_0 (molecules)	η^0 (10^{-6})	θ_0 (K)	β (K s^{-1})	T_P^0 (K)		T_P^+ (K)		θ_P^0 (ML)		θ_P^+ (ML)		D_P^0 (ML s^{-1})		D_P^+ ($\times 10^{-4}$ ML s^{-1})		ε_P^+ ($\times 10^{-2}$)	
					P_1^0	P_2^0	P_1^+	P_2^+	P_1^0	P_2^0	P_1^+	P_2^+	P_1^0	P_2^0	P_1^+	P_2^+	P_1^+	P_2^+
Fig. 9																		
1	6.02×10^{12}	–	0.366	3.2	677	1091	915	1162	0.32	0.03	0.11	0.01	0.002	0.001	2.74	0.80	8.95	16.3
2	6.02×10^{13}	–	3.53	3.2	685	1130	940	1124	2.70	0.68	1.46	0.72	0.047	0.016	1.04	1.70	1.73	0.98
3	6.02×10^{14}	–	35.3	3.2	689	1082	934	1196	13.3	5.03	9.47	4.43	0.169	0.11	0.61	10.7	0.22	0.97
4	6.02×10^{15}	–	353	3.2	683	1100	–	1154	159	18.9	–	12.7	8.26	0.32	–	15.3	–	0.55
5	6.02×10^{16}	–	3530	3.2	709	–	–	1169	1261	–	–	18.6	72.5	133	–	6.33	–	0.17
Fig. 10																		
1	6.02×10^{14}	30.4	28.2	0.76	589	967	910	1030	22.3	14.0	14.3	13.7	0.15	0.005	0.05	1.11	0.125	3.86
2	6.02×10^{14}	34.8	28.2	1.02	595	980	924	1041	23.2	16.7	17.2	16.2	0.14	0.010	0.07	1.70	0.105	3.29
3	6.02×10^{14}	8.9	28.2	3.19	608	990	923	1087	16.7	1.36	1.95	0.69	1.05	0.031	0.23	2.12	0.097	1.98
4	6.02×10^{14}	6.7	28.2	22.2	681	1112	972	1101	14.4	1.37	2.83	1.51	6.44	0.289	0.61	1.93	0.097	0.071
5	6.02×10^{14}	11.8	28.2	66.6	704	1164	872	1122	18.2	2.17	5.27	2.86	14.6	0.116	3.03	5.85	0.032	0.057

Table 6
Summary of the activation energies (E^0 and E^+ in kJ/mol) and frequency factors (ν^0 and ν^+ in s^{-1}) for neutral and ionic desorptions from LiX/Pt systems (here, E_s^0 is the sublimation heat (in kJ/mol) cited from literature)

Sample	θ_0 (ML)	E_s^0	Molecule (LiX^0)			Ion (Li^+)		
			P_1^0	P_2^0	P_3^0	P_1^+	P_2^+	P_3^+
E (kJ mol^{-1})								
LiF	12.8	270	220 ± 5	–	–	167 ± 5	–	–
	128		281 ± 12	396 ± 16	–	196 ± 29	326 ± 14	–
LiCl	20.4	206	135 ± 1	–	–	–	286 ± 2	–
	210		145 ± 6	277 ± 13	–	–	291 ± 7	234 ± 8
	2105		205 ± 8	365 ± 11	–	–	–	–
LiBr	22.5	190	139 ± 3	344 ± 2	377 ± 2	375 ± 2	535 ± 5	–
LiI	28.2	172	121 ± 2	–	–	–	406 ± 7	–
ν (s^{-1})								
LiF	12.8	–	1.2×10^{17}	–	–	7.8×10^{10}	–	–
	128		5.3×10^{15}	3.1×10^{16}	–	4.7×10^{10}	4.0×10^{13}	–
LiCl	20.4	–	8.8×10^{8}	–	–	–	3.9×10^{14}	–
	210		3.9×10^{9}	4.3×10^{11}	–	–	3.2×10^{12}	1.1×10^{9}
	2105		2.6×10^{13}	2.8×10^{15}	-	–	–	–
LiBr	22.5	–	4.7×10^{9}	5.8×10^{14}	6.6×10^{15}	1.4×10^{16}	5.1×10^{18}	–
LiI	28.2	–	2.1×10^{9}	–	–	–	1.6×10^{19}	–

usually equal to the image force [10] given by

$$E_i^+ = \frac{e^2}{4r} = 571 \text{ kJ/mol}. \quad (6)$$

Here, e is the elementary electric charge and r is the radius of Li^+ (6.07×10^{-9} cm) [11]. Compared with $E_i^+ = 571$ kJ/mol, any value of $E_1^+ - E_3^+$ is very small (167–535 kJ/mol, see Table 6). This may be quite natural because the peaks ($P_1^+ - P_3^+$) employed to determine $E_1^+ - E_3^+$ appear usually at $\theta_P^+ > 1$ ML (see Table 2 and the lower halves of Tables 3–5). In other words, Li^+ is desorbed not from an essentially bare surface of the base metal (Pt) but from the active sites of LiX with high work function, which will be described in Section 3.4. In Table 1 and the upper halves of Tables 3–5 (especially row 1 corresponding to $\theta_0 \leq 1$ ML), on the other hand, some of $P_1^+ - P_3^+$ are found to appear at $\theta_P^+ < 1$ ML. In this case, Li^+ is desorbed mainly from the surface not of LiX but of Pt. At $\theta_0 \leq 1$ ML, however, it is very difficult for a TPD method to determine E^+ correctly.

3.3. Effective concentration

Consideration of our experimental data from the viewpoint of chemical kinetics leads to

$$D_P^{0+} = A_P^{0+} \nu^{0+} \exp[-E^{0+}/RT_P^{0+}]. \quad (7)$$

Here, A_P^{0+} is the sample amount (effective concentration) actually participating in the neutral or ionic desorption at the peak appearance temperature (T_P^0 or T_P^+). In the case of LiF at $\theta_0 = 128$ ML and $\beta = 3.4$ K, for example, $A_{P_1}^0$ corresponding to P_1^0 is evaluated from Eq. (7) to be 22.5 ML since $D_{P_1}^0 = 5.17$ ML and at $T_{P_1}^0 = 900$ K (see row 1 in Table 2) and since $E_1^0 = 281$ kJ/mol and $\nu_1^0 = 5.3 \times 10^{15}$/s (see rows 2 and 8 in Table 6). On the other hand, $\theta_{P_1}^0$ is 52.6 ML (see row 1 in Table 2) and hence $A_{P_1}^0/\theta_{P_1}^0$ is evaluated to be 0.43 (see row 1 in Table 7). Consequently, the LiF molecules included in the upper layers (43%) alone participate in the neutral desorption, and only those molecules (23% of $A_{P_1}^0$) satisfying $E_1^0 \geq 281$ kJ/mol (see row 2 in Table 6) are desorbed from the crystal state as LiF^0 at the rate ($D_{P_1}^0$) of 5.17 ML/s at $T_{P_1}^0 = 900$ K, thus giving P_1^0.

With respect to P_1^+ in the same run, $A_{P_1}^+$ and $A_{P_1}^+/\theta_{P_1}^+$ are evaluated to be 8.7×10^{-5} ML and 9.0×10^{-7} (see row 1 in Table 7), respectively, although $\theta_{P_1}^+$ is as large as 97.1 ML (see row 1 in Table 2). Consequently, Li^+ is desorbed from the active sites (high work function spots) of LiF itself, and $A_{P_1}^+/\theta_{P_1}^+$ may be considered to represent the fractional surface area at $T_{P_1}^+ = 861$ K. After thermal dissociation ($LiF \rightarrow Li + F$) and ionization ($Li \rightarrow Li^+ + e$) on the active sites, only those ions ($\sim$10% of $A_{P_1}^+ = 8.7 \times 10^{-5}$ ML

Table 7
Effective amounts or "effective concentrations" (A_P^0 and A_P^+) of LiX participating in neutral and ionic desorptions and their relative values (A_P^0/θ_P^0 and A_P^+/θ_P^+) to the actual amounts or "actual concentrations" (θ_P^0 and θ_P^+) present on the platinum surface at respective peak temperatures (T_P^0 and T_P^+) listed in Tables 2–5 (see Figs. 4–10)

LiX	Curve	θ_0 (ML)	β (K s^{-1})	A_P^0 (ML)			A_P^0/θ_P^0			A_P^+ ($\times 10^{-4}$ ML)			A_P^+/θ_P^+ (10^{-3})		
				P_1^0	P_2^0	P_3^0	P_1^0	P_2^0	P_3^0	P_1^+	P_2^+	P_3^+	P_1^+	P_2^+	P_3^+
LiF (Fig. 4)															
	1	128	3.4	22.5	13.4	–	0.43	~1	–	0.87	21.8	–	0.0009	0.20	–
	2	128	7.9	31.6	3.0	–	0.62	0.59	–	–	5.3	–	–	0.10	–
	3	128	20.0	34.4	2.4	–	0.56	0.41	–	2.12	11.1	–	0.0039	0.16	–
	4	128	29.8	21.0	6.1	–	0.30	0.55	–	1.72	12.6	–	0.0025	0.090	–
	5	128	57.4	25.8	5.5	–	0.39	0.47	–	6.52	8.4	–	0.010	0.059	–
	6	128	139.6	9.0	–	–	0.13	–	–	–	4.9	–	–	0.028	–
Mean		–	–	24 ± 8	6.1 ± 3.9	–	0.41 ± 0.16	~6		2.8 ± 2.2	10.7 ± 5.7	–	0.0044 ± 0.0035	0.11 ± 0.06	–
LiCl (Fig. 6)															
	2	210	3.7	44	9.2	–	0.46	~0.8	–	–	48	36	–	0.37	0.92
	3	210	14.6	47	12	–	0.44	~1	–	–	5.3	4.2	–	0.031	0.25
	4	210	29.1	53	12	–	0.48	~1	–	–	2.5	1.9	–	0.017	0.11
	5	210	57.3	66	15	–	0.55	~0.9	–	–	1.3	1.2	–	0.006	0.35
Mean		–	–	53 ± 8	12 ± 2	–	1.9 ± 0.5	~1	–	–	14 ± 20	11 ± 15	–	0.11 ± 0.15	0.41 ± 0.31
LiBr (Fig. 8)															
	1	22.5	0.36	5.7	1.3	1.4	0.37	0.31	0.51	280	430	–	7.4	20	–
	2	22.5	0.81	2.7	1.8	1.5	0.18	0.35	0.50	240	480	–	5.4	19	–
	3	22.5	1.20	3.0	1.5	1.7	0.20	0.42	0.80	270	360	–	8.5	23	–
	4	22.5	3.60	6.6	1.1	1.1	0.41	0.26	0.40	150	240	–	4.0	10	–
	5	22.5	7.40	7.5	1.3	1.0	0.53	0.39	0.43	250	360	–	7.5	15	–
	6	22.5	23.8	5.1	–	3.2	0.33	–	0.87	–	320	–	–	6	–
Mean		–	–	5.1 ± 1.8	1.4 ± 0.2	1.7 ± 0.7	0.34 ± 0.12	0.35 ± 0.06	0.59 ± 0.18	240 ± 50	370 ± 80	–	6.6 ± 1.6	16 ± 6	–
LiI (Fig. 10)															
	1	28.2	0.75	1.7	–	–	0.078	–	–	–	98.2	–	–	0.72	–
	2	28.2	1.02	1.3	–	–	0.058	–	–	–	91.3	–	–	0.56	–
	3	28.2	3.2	5.9	–	–	0.351	–	–	–	15.6	–	–	2.25	–
	4	28.2	22.2	4.1	–	–	0.287	–	–	–	8.0	–	–	0.53	–
	5	28.2	66.6	3.1	–	–	0.168	–	–	–	10.5	–	–	0.37	–
Mean		–	–	3.2 ± 1.7	–	–	0.19 ± 0.18	–	–	–	45 ± 41	–	–	0.89 ± 0.62	–

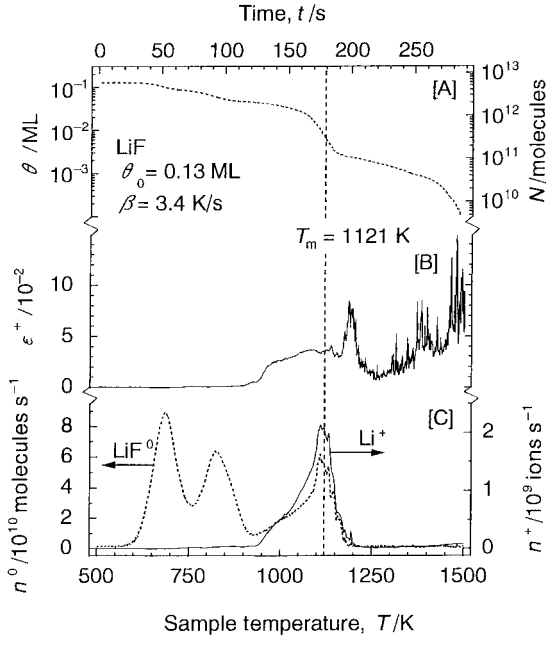

Fig. 12. Temperature of LiF ($\theta_0 = 0.13$ ML) vs. (A) the sample layer thickness (θ) on Pt, (B) the ionization efficiency ($\epsilon^+ \approx n^+/n^0$) and (C) the neutral or ionic desorption rate (n^0 or n^+) measured at $\beta = 3.4$ K/s (see row 1 in Table 1).

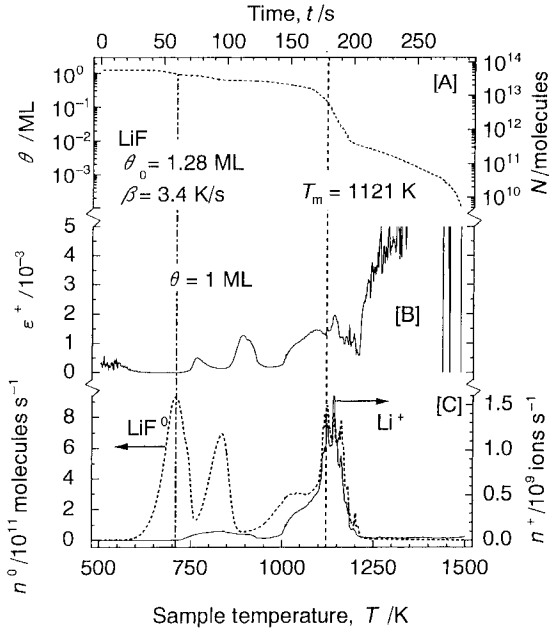

Fig. 13. Temperature dependence of (A) the thickness (θ) of LiF ($\theta_0 = 1.28$ ML), (B) the efficiency (ϵ^+) and (C) the desorption rates (n^0 or n^+) at $\beta = 3.4$ K/s (see row 2 in Table 1).

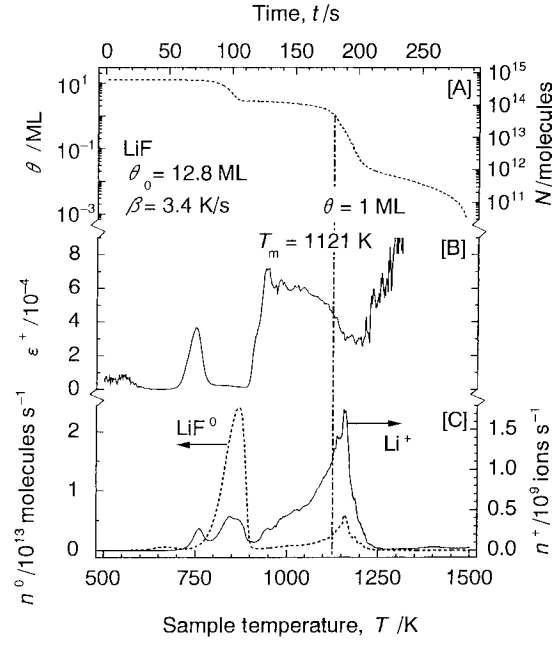

Fig. 14. Temperature dependence of θ, ϵ^+, n^0 and n^+ measured with LiF ($\theta_0 = 12.8$ ML) at $\beta = 3.4$ K/s (see row 3 in Table 1).

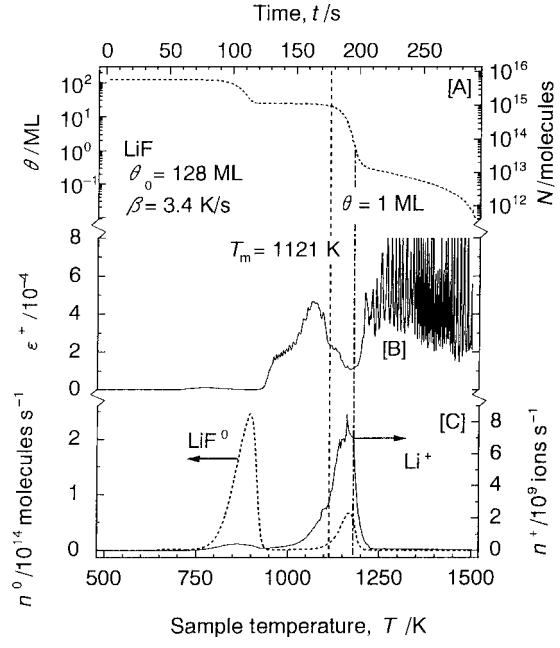

Fig. 15. Temperature vs., θ, ϵ^+, n^0 and n^+ determined with LiF ($\theta_0 = 128$ ML) at $\beta = 3.4$ K/s (see row 4 in Table 1).

Table 8
Summary of our experimental data (E^0, E^+ and ϕ^+ in kJ/mol and $S_a \equiv A_P^+/\theta_P^+$, ϵ^+, etc.) and literature values ($D^=$ and I in kJ/mol)

LiX (θ_0 in ML)	Peaks	T (K)	θ_P^+ (ML)	$D^=$ (kJ mol^{-1})	I (kJ mol^{-1})	E^0 (kJ mol^{-1})	E^+ (kJ mol^{-1})	ϕ^+ (kJ mol^{-1})	S_a	$\bar{S}_a$	ϵ^+	$\bar{\epsilon}^+$
LiF (128)	P_2^0 and P_2^+	1162–1297	5–17	588	546	396 ± 18	326 ± 14	878 ± 33	2×10^{-4}–3×10^{-5}	$(1.1 \pm 0.6) \times 10^{-4}$	4×10^{-5}–1×10^{-4}	$(9 \pm 3) \times 10^{-5}$
LiCl (210)	P_2^0 and P_2^+	1010–1294	8–23	485	544	277 ± 13	291 ± 7	724 ± 19	4×10^{-4}–6×10^{-6}	$(1.1 \pm 1.5) \times 10^{-4}$	1×10^{-3}–8×10^{-6}	$(3 \pm 4) \times 10^{-4}$
LiBr (22.5)	P_2^0 and P_1^+	1082–1164	3–5	431	544	344 ± 2	375 ± 2	569 ± 4	4×10^{-3}–9×10^{-3}	$(6.6 \pm 1.6) \times 10^{-3}$	3×10^{-2}–2×10^{-2}	$(2 \pm 1) \times 10^{-2}$

$= 4.1 \times 10^9$ ions) satisfying $E_1^+ \geq 196$ kJ/mol (see row 2 in Table 6) are desorbed from the sites as Li^+ at the rate of $D_{P_1}^+ = 8.8 \times 10^{-6}$ ML/s $= 4.1 \times 10^8$ ions/s at $T_{P_1}^+$ (see row 1 in Table 2).

Quite similarly as above, both A_P^0 and A_P^+ were determined with other peaks (P_2^{0+}) of LiF and also with all the peaks of the other halides, too. The results thus achieved are summarized in Table 7, indicating that the fractional surface area (A_P^+/θ_P^+) of the active sites promoting the desorption of Li^+ is at the most ca. 2% at P_2^+ of LiBr and at the least ca. 9×10^{-5}% at P_1^+ of LiF. In other words, more than 98% of the desorbing surface consist of non-active sites with low work function and hence promote the desorption of LiX^0.

3.4. Ionization efficiency and work function

Temperature dependence of the ionization efficiency (ϵ^+) observed with LiF ($\theta_0 = 0.13$–128 ML) are shown in Figs. 12–15, which include the relation between T and θ, too. As θ_0 increases, ϵ^+ tends to decrease from ca. 10^{-2} to 10^{-4} at any temperature. It should be noted that ϵ^+ becomes generally larger at $\theta < 1$ ML. When θ_0 is less than ca. 1 ML or when θ becomes less than ca 1 ML at high temperatures above T_m, Li^+ is generally desorbed from the surface of Pt. Even at $\theta >> 1$ ML, however, Li^+ can be desorbed from those active sites on the layers of LiX itself. As shown in Table 2, $\theta_{P_1}^+$ is as large as 97–55 ML, but Li^+ is desorbed at $D_{P_1}^+ \geq 10^{-5}$ ML/s. The work function (ϕ^+) of the sites can be evaluated [12] from

$$\phi^+ = I + D^= + E^0 - 2E^+. \quad (8)$$

Here, I is the ionization energy of Li and $D^=$ is the dissociation energy of LiX, readily obtainable from thermochemical tables [9]. In the case of LiF ($\theta_0 = 128$ ML and $\beta = 3.4$–140 K/s, see Table 2), each peak of P_2^+ appears at $T_{P_2}^+ = 1162$–1276 K, well overlapping with $T_{P_2}^0 = 1168$–1297 K. In addition, $\theta_{P_2}^+$ and $\theta_{P_2}^0$ are in the ranges of ca. 5–17 and 5–13 ML, respectively, much larger than 1 ML. Therefore, each P_2^+ originates from those active sites and hence ϕ^+ is evaluated from Eq. (8). Typical results thus obtained are summarized in Table 8. Here, $\bar{S}_a$ is the mean value of the fractional surface area ($S_a \equiv A_P^+/\theta_P^+$) of the active sites affording the peak of P_2^+ or P_1^+. It should be noted that ϵ^+ is strongly governed by both ϕ^+ and S_a and also that ϕ^+ depends upon E^0 and $D^=$. This is the main reason why ϵ^+ and its mean value ($\bar{\epsilon}^+$) rang from ca. 10^{-5} to ca. 10^{-2} depending upon the species of LiX.

4. Conclusion

The above experimental data and analytical results achieved with LiF–LiI yield the conclusions as follows. (1) The first peak (P_1^0) appearing below T_m of each LiX is partly due to the desorption from physical adsorption state of LiX. (2) The other peaks (P_2^0 and P_3^0) above T_m originates from the chemisorption states of LiX. (3) Those ionic peaks ($P_1^+ - P_3^+$) appearing at $\theta >> 1$ ML are due to the desorption from the active sites on LiX itself, while those at $\theta \leq 1$ ML originate from the ion desorbed from the surface of Pt. (4) The mean fractional surface area ($\bar{S}_a$) of the active sites on LiX ranges from ca. 6×10^{-6} to 9×10^{-3}, depending upon the species of LiX. (5) The work function (ϕ^+) of the sites also depends upon the species of LiX, ranging from 878 to 569 kJ/mol.

However, much work is necessary to clarify both physical structure and chemical composition of the active sites and also to examine the effect of the base metal upon the ionic desorption especially at high temperatures above T_m of each sample.

References

[1] H. Kawano, Mass Spectrosc. 22 (1974) 251.
[2] H. Kawano, S. Kamidoi, H. Shimizu, Rev. Sci. Instrum. 67 (1996) 1387.
[3] H. Kawano, S. Kamidoi, H. Shimizu, K. Ushimaru, H. Asada, Appl. Surf. Sci. 100/101 (1996) 174.
[4] H. Kawano, Y. Zhu, S. Kamidoi, H. Shimizu, M. Udaka, Thermochim. Acta 299 (1997) 59.
[5] Y. Zhu, T. Maeda, H. Kawano, Stud. Surf. Sci. Catal. 112 (1997) 377.
[6] H. Kawano, T. Kenpô, Y. Hidaka, Int. J. Mass Spectrom. Ion Proc. 62 (1984) 137.
[7] H. Kawano, K. Ogasawara, H. Kobayashi, A. Tanaka, T. Takahashi, Y. Tagashira, Rev. Sci. Instrum. 69 (1998) 1182.
[8] P.A. Redhead, Vacuum 12 (1962) 203.
[9] M.W. Chase, Jr., C.A. Davis, J.R. Downey, Jr., D.F. Frurip, R.A. McDonald, A.N. Syverd, JANAF Thermochemical Tables, 3 ed., American Chemical Society and American Institute of Physics, New York, 1985.
[10] H. Inouye, H. Kawano, Appl. Phys. (Jpn.) 38 (1969) 1145.
[11] L. Pauling, The Nature of the Chemical Bond, 3 ed., Cornell University Press, Ithaca, NY, 1960 p. 526.
[12] H. Kawano, T. Kenpô, Int. J. Mass Spectrom. Ion Proc. 54 (1983) 127.